





## An Efficient Algorithm for Detecting Flatness of Small Metal Parts Based on Stereo Matching of Multi-Similarity Fusion

Liangang Xie<sup>1</sup> , Xianda Li<sup>2</sup>  and Xiangzhi Wei<sup>3</sup> 

<sup>1</sup>Shanghai Jiao Tong University, [liangangxie@sjtu.edu.cn](mailto:liangangxie@sjtu.edu.cn)

<sup>2</sup>Shanghai Jiao Tong University, [sbnine@sjtu.edu.cn](mailto:sbnine@sjtu.edu.cn)

<sup>3</sup>Shanghai Jiao Tong University, [antonwei@sjtu.edu.cn](mailto:antonwei@sjtu.edu.cn)

Corresponding author: Xiangzhi Wei, [antonwei@sjtu.edu.cn](mailto:antonwei@sjtu.edu.cn)

**Abstract.** Metal covers for the electronic chips are required to be flat upon a maximum error of 0.1mm such that they can be pasted to flat zones of the printed circuit boards stably. These metal covers are cheap and widely used, and they require a fast flatness test in order to save production time and cost. The existing non-contact flatness measurement methods are based on dense surface reconstruction, which induces unnecessary noise and processing time. For thin parts with a thickness of less than 2 mm, an efficient scheme based on binocular stereo vision is proposed to detect the flatness by reconstructing the boundaries of the parts instead of the entire surface of the parts. To reduce the measurement errors and speed up the detection process, we propose a hybrid strategy to detect the 2D boundaries by combining Canny operator, Zernike moment operator and linear interpolation to achieve subpixel-level precision efficiently. Moreover, a stereo matching algorithm based on a similarity fusion of shape, gradient and disparity is proposed to achieve precise matching. A calibration method is introduced to calibrate the supporting plane for the parts with specially designed markers. The methodology was tested on a set of thin metal covers, and a comparison with the laser profiler and the structured light method was conducted to validate its effectiveness. The experimental results showed that our proposed method has nice precision and efficiency for small metal covers.

**Keywords:** Boundary Detection, Flatness Measurement, Stereo Matching, Metal Parts.

**DOI:** <https://doi.org/10.14733/cadaps.2021.571-583>

### 1 INTRODUCTION

With the rapid development of mobile phones, GPS and other electronic communication equipment, the demand of metal covers for their Printed Circuit Boards (PCB) is also growing. Metal covers are mainly used to shield electromagnetic interference to protect electronic chips. The

metal covers for electronic chips are usually small in size (e.g., with a side-width less than 20 mm and a thickness less than 2 mm). However, due to their low stiffness, metal covers are easily deformed in the process of production, transportation, sorting and packaging. Therefore, it is necessary to detect their flatness and eliminate the deformed ones before pasting them onto the PCB.

Existing flatness measurement techniques are mainly non-contact, i.e., no physical contacts occur between the measuring device and the parts. Compared with contact measurement approaches, non-contact measurement approaches have the advantage of high efficiency. These approaches include time-of-flight technique (ToF), laser sensor, structured light technique, etc., and they vary in measurement sensitivity, resolution and measurement ranges.

Many researchers have applied 3D laser technologies to flatness measurement. For example, Wang et al. [15] introduced recent technological advances in 3D laser technologies for detecting road flatness. Molleda et al. [11] reviewed various flatness detection technologies (e.g., 3D laser sensors) in the iron and steel industry. Wang et al. [16] applied the laser scanning technology to inspect surface flatness on precast concrete elements. However, the laser profiler needs the help of a high-precision sliding guide to scan through the measured surface, and the moving process is time-consuming when measuring little parts.

TOF has also been widely used in 3D field due to its measuring speed. For example, Guomundsson et al. [6] applied ToF cameras in segmenting foreground objects from the background. Cui et al. [4] proposed a novel method by combining a 3D super-resolution method and a probabilistic scan alignment approach to significantly reduce the noise of point clouds generated by ToF. However, due to their low resolution, ToF devices are mostly used for rough 3D measurements.

Structured light has the advantage of high measurement accuracy, which has also been widely explored. For example, Lilienblum et al. [9] proposed a novel technique for optical 3D surface reconstruction by using line-scan cameras and structured light in combination and achieved a high-quality surface reconstruction. Le et al. [8] proposed an innovative algorithm for reconstructing a 3D surface profile with a sharp-boundary using multi-dimensional data fusion. But structured light devices need to project coded stripe images on the scanned surface, which may generate reflections on the boundaries of metal parts. The reflections can induce large noise or absence of point cloud.

Stereo vision technology has been widely used in robot vision guidance, 3D perception of unmanned cars, rough 3D measurement, etc. For example, Aguilar et al. [1] evaluated the accuracy of different camera calibration and measurement methods used in 3D stereo vision and applied stereo vision technology in car frame measurement. Kieu et al. [7] proposed a full-field 3D shape measurement method with high accuracy in the presence of discontinuities and multiple separate regions. However, due to the monotonous surface texture and sparse features of metal parts, the conventional binocular stereo vision equipment is sensitive to noise in the process of stereo matching.

In this paper, we propose a boundary reconstruction algorithm based on binocular vision to detect the flatness of metal parts. Different from the conventional binocular stereo vision and structured light approaches, we only reconstruct the boundary points of the metal part instead of the entire surface.

The main contributions of this paper include the following three aspects.

- A flatness measurement scheme based on a boundary reconstruction (instead of the entire 3D surface) algorithm is designed for high-resolution flatness measurement. The proposed scheme has obvious advantages of high-speed and low-cost without using any additional mechanism or projection equipment.
- A hybrid subpixel-boundary detection algorithm based on Canny, Zernike and linear interpolation is proposed to obtain more precise boundary coordinates, which is convenient for fast and accurate line-by-line stereo matching.

- A stereo matching algorithm based on a similarity fusion of shape, gradient and disparity is proposed for the stereo matching of boundary points. The algorithm mitigates the mismatch error due to the similar textures and colors on the same horizontal line of a pair of images.

The remainder of this paper is organized as follows. Section 2 introduces the methodology; Section 3 presents the experimental results and a comparison with other methods; finally, Section 4 concludes the paper with some discussions.

## 2 METHODOLOGY

### 2.1 The Boundary Reconstruction Strategy

The procedure of boundary reconstruction based on binocular vision technology is shown in Figure 1(a).

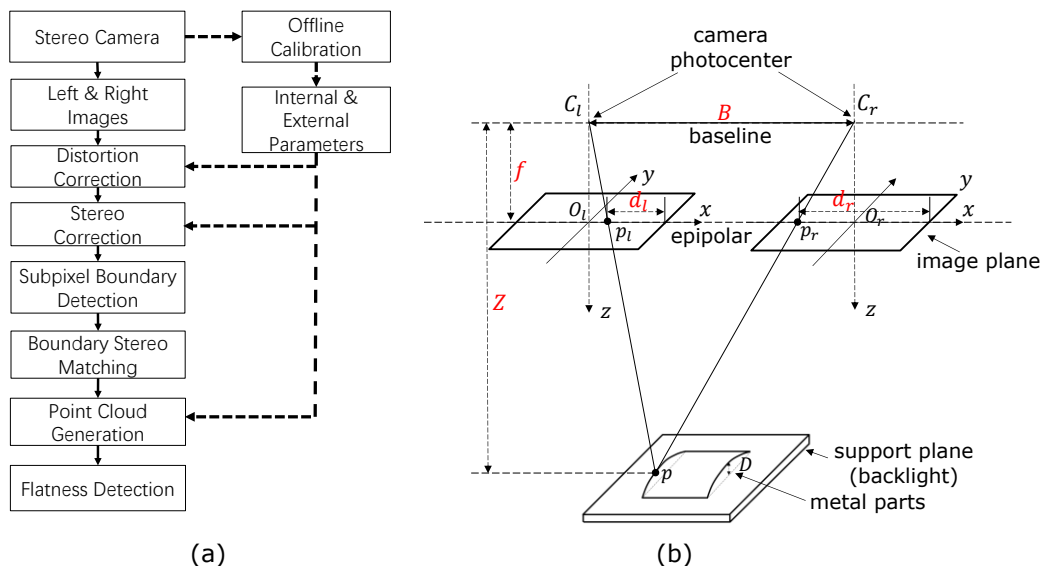


**Figure 1:** (a) Flow chart of 3D boundary reconstruction scheme, (b) a schematic diagram of binocular vision system.

As shown in Figure 1(b), after the process of distortion correction and stereo correction, two image planes are transformed to the same plane and the epipolar lines of two image planes are adjusted to the same row. According to the epipolar constraint criterion [13], only one-dimensional search on the same line is needed to match the corresponding points.

In Figure 1(b),  $P$  is a boundary point of the metal part.  $p_l$  and  $p_r$  are projections of  $P$  on left and right image planes respectively. The problem is reduced to matching  $p_l$  and  $p_r$  accurately and efficiently. Based on the results of calibration, the coordinates  $(X, Y, Z)$  corresponding to pixel  $(u, v)$  can be obtained. According to the triangle principle, the distance  $Z$  between the object point  $P$  and the camera baseline satisfies Equation (1.1) and Equation (1.2)[10].

$$\frac{Z-f}{B-(d_r-d_l)} = \frac{Z}{B} \quad (1.1)$$

$$Z=Bf/D(d), \text{ where } D(d)=d_r-d_l \quad (1.2)$$

where  $B$  is the length of the baseline and  $f$  is the focal length, which are obtained in the calibration process;  $d_l$  and  $d_r$  are the  $x$ -coordinates of the corresponding points  $p_l$  and  $p_r$ , respectively;  $D(d)$  is the *disparity* of  $d_l$  and  $d_r$ .

After obtaining the depth  $Z$ ,  $X$  and  $Y$  can also be obtained by Equation (1.3).

$$\begin{cases} X = (u - c_x) \cdot Z / f_x \\ Y = (v - c_y) \cdot Z / f_y \end{cases}, \text{ where } f_x = f / S_x, f_y = f / S_y \quad (1.3)$$

where  $c_x$  and  $c_y$  are the pixel coordinates of the center pixel of an image,  $S_x$  and  $S_y$  are the horizontal and vertical side-lengths of a pixel respectively. Thereafter, the coordinates  $(X, Y, Z)$  of each boundary point can be obtained. Thereafter, we calculate the number of neighboring points for each point in a circle with fixed radius. Any point whose neighboring points are less than a user-defined threshold is considered as an outlier and should be eliminated. The remaining points may participate in the calculation of flatness, and these points are called *valid points*. Subsequently, we calibrate the support plane and detect the flatness of the part by calculating the heights of valid points w.r.t the calibrated support plane.

## 2.2 A Hybrid Subpixel-Boundary Detection Algorithm

### 2.2.1 A hybrid of Canny, Zernike and linear interpolation

In order to reconstruct the 3D coordinates of the boundary points, the 2D boundary detection should be conducted on the image to obtain the 2D coordinates of the boundary. The precision of 2D boundary detection directly affects the quality of the resultant 3D coordinates. Boundary detection algorithms focus on pixel-level and subpixel-level precisions [10]. The subpixel boundary detection algorithms can overcome the limits of the physical resolution of CCD cameras and achieve an extremely high precision [12]. However, if a subpixel detection algorithm is applied to each pixel, it will be extremely time-consuming and unsuitable for industrial applications with real-time requirements [3]. In order to balance the efficiency and accuracy, we combine Canny with Zernike and take their respective advantages. Refer to Figure 2, the Canny operator is first used to detect the green integer pixel point; and then the Zernike operator is applied to detect the blue subpixel points (to be shown in Section 2.2.2). Since the stereo matching matches the points on the same row from the left and the right images, a linear interpolation is applied to obtain the resultant subpixel points (orange) based on the horizontal lines of the pixel map and the boundary curve (blue) derived by the Zernike operator.

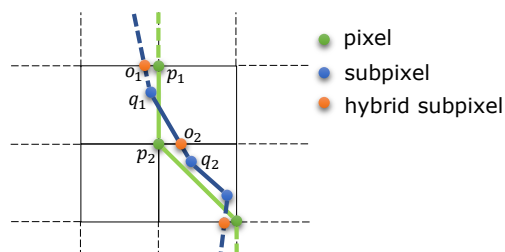


**Figure 2:** Deriving subpixel points (orange) from the Canny operator (green), and Zernike operators (blue) in sequence.

### 2.2.2 Zernike subpixel boundary detection algorithm

The Zernike operator is applied to calculate more accurate subpixel boundary points based on the local grayscale information of a circular area. Refer to Figure 3(a), the circular area can be divided

into two parts with different gray values by the boundary. Because its 3D diagram is like a step, the circular area of an edge point can be abstracted into a step model defined by multiple parameters. More specifically, let  $O$  be the center of the circle on top of the lower cylinder; let  $b$  and  $h$  be the heights of the lower and upper cylinders respectively, which indicate the gray levels of the two sides of a boundary  $L$  (Figure 3 (b)).  $O$  can be derived from the Canny operator, but its precision is at a pixel-level and it may be a little bit away from the real boundary  $L$  [2]; to obtain a subpixel-level point on the boundary (instead of  $O$ ), the Zernike operator is applied to compute a point  $P$  that is closest to  $O$  by using the information of  $h, b, \theta$  and  $d$  in sequence by applying Equation (2.1-2.5) [5][14].

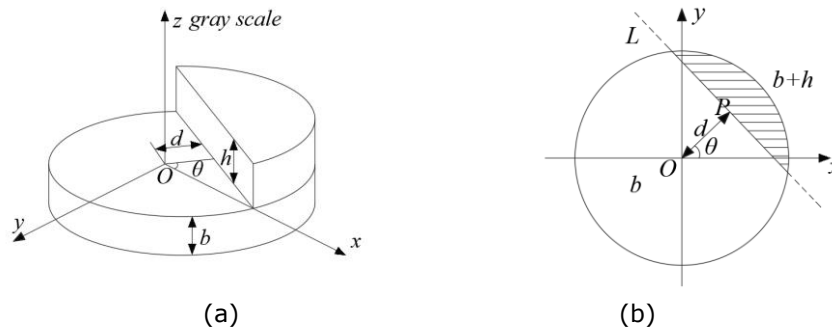


**Figure 3:** Step model for sub-pixel boundary. (a) Three-dimensional step model diagram, (b) Two-dimensional step model diagram.

$$h = 3Z'_{11} \left[ 2(1-d^2)^{3/2} \right]^{-1} = 3Z_{11} \left[ 2(1-d^2)^{3/2} \right]^{-1} e^{j\theta} \quad (2.1)$$

$$b = \left[ Z_{00} - \frac{h\pi}{2} + h \sin^{-1}(d) + hd(1-d^2)^{\frac{1}{2}} \right] / \pi \quad (2.2)$$

$$\theta = \arctan(\text{Im}[Z_{11}] / \text{Re}[Z_{11}]) \quad (2.3)$$

$$d = Z_{20} / Z'_{11} = Z_{20} e^{-j\theta} / Z_{11} \quad (2.4)$$

$$\begin{bmatrix} x_s \\ y_s \end{bmatrix} = \begin{bmatrix} x \\ y \end{bmatrix} + \frac{N}{2} d \begin{bmatrix} \cos\theta \\ \sin\theta \end{bmatrix} \quad (2.5)$$

where  $N$  represents the number of pixels inside the square enclosing the Zernike circle [5].

After processing each integer pixel (e.g., point  $O$  in Figure 3) obtained by the Canny operator, a set of sub-pixel coordinates of the boundary can be obtained by applying Equation (2.1-2.5) in sequence. Figure 4 shows an example of the subpixel boundary points obtained from the right image (corresponding to the right camera).

### 2.3 Similarity Fusion of Shape, Gradient and Disparity

As mentioned above, matching the corresponding points of left and right images accurately and efficiently is a challenge in 3D measurement. For example, in Figure 5, the red dots on the right image are candidate points that may match the same green dot on the left image. Therefore, a robust similarity measurement is required to evaluate the similarity of each pair of matching points. Unlike traditional dense stereo matching, in our task the boundary points to be matched

are sparse, non-integral and lack of color information, which increase the difficulties of precise matching since their shape and texture features are highly similar.

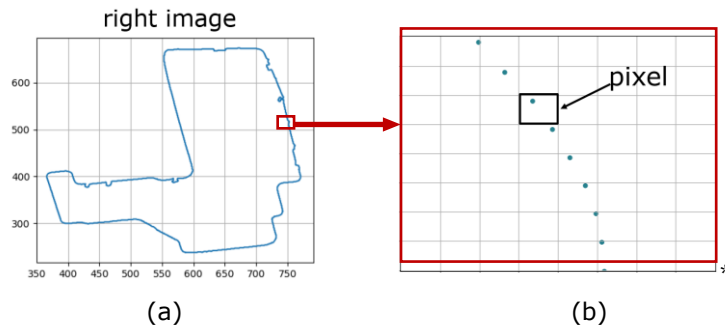


**Figure 4:** (a) Sub-pixel boundary points on the right image, (b) a close-up look of a small portion on the right image.

To address this issue, we propose a similarity fusion of shape, gradient and disparity to calculate the matching information at each pair of points.

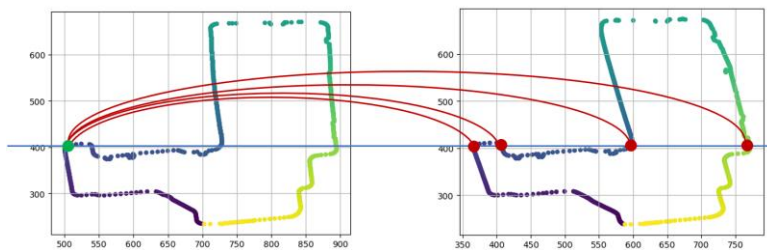


**Figure 5:** One point on the left image may be mismatched to a set of points on the right image

For ease of computation, for each boundary point, we create a window centered at this point with its nearest neighboring integer pixels included in the window. The size of the window is  $N$ , where  $N$  can be adjusted to increase/reduce the number of neighboring pixels used for computation.

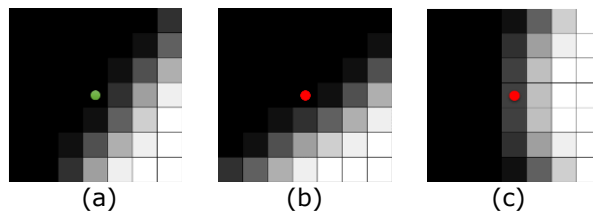


**Figure 6:** (a) A window at a point on the left image, (b) and (c): windows at two different points on the right image.

Figure 6(a) is a window of a point (green) in the left image. Figure 6(b) and (c) are the windows of two points (red) of the right image. It can be seen intuitively that (b) is more similar to (a) than (c). In order to describe this kind of similarity, as shown in Equation (2.6), the square sum of the difference of the gray values in the corresponding positions of two windows is used.

$$C_{SSD}(p, d) = \sum_{s=1}^N \sum_{t=1}^N [I_R(s, t) - I_L(s, t)]^2 \quad (2.6)$$

where  $I_L$  is the gray value of left pixel  $p$  and  $I_R$  is the gray value of right pixel  $q$ . And  $d$  is the difference of the x-coordinates of the current pair of points to be matched, which is usually called *disparity*. When the difference between the gray values of two windows is large,  $C_{SSD}(p, d)$  is also large. Note that  $C_{SSD}(p, d)$  is sensitive to the shape difference of the distribution of the neighborhood of a point at the center of the left image and that of another point at the center of the right image, so we call it *shape similarity measurement*.

Although  $C_{SSD}(p, d)$  can describe the similarity of shapes, it is sensitive to random noise and overall difference of brightness of two cameras. To mitigate this, we further exploit the gradient information of the points. Based on the results of Zernike operator, a similarity measurement for boundary gradients is proposed in Equation (2.7). This equation combines the amplitude component and angle component of the gradient calculated by integral of Zernike, and thus is very robust to noise and illumination changes.

$$C_{dir}(p, d) = (\|\vec{p}\| - \|\vec{q}\|) / (k * (\|\vec{p}\| + \|\vec{q}\|) * (\cos\langle\vec{p}, \vec{q}\rangle + \sigma)) \quad (2.7)$$

where  $\|\vec{p}\|$  and  $\|\vec{q}\|$  denote the average gradient amplitudes of all subpixel edge points in the window of left pixel  $p$  and right pixel  $q$  respectively, and they can be expressed as the average gray step value  $h_L$  and  $h_R$  of all points in the window centered on  $p$  and  $q$  respectively; angle  $\langle\vec{p}, \vec{q}\rangle$  is the difference of the angle of the average gradient direction of all points in the window;  $k$  is a coefficient used to measure the relative importance of the gradient amplitude to the angle, and  $k > 0$ ;  $\sigma$  is a correction factor that ensures the denominator is positive, and  $\sigma > 1$ .

$$C_{dir}(p, d) = \left( \frac{1}{n_L} \sum_{i=1}^{n_L} h_{Li} - \frac{1}{n_R} \sum_{i=1}^{n_R} h_{Ri} \right) / \left( k * \left| \frac{1}{n_L} \sum_{i=1}^{n_L} h_{Li} + \frac{1}{n_R} \sum_{i=1}^{n_R} h_{Ri} \right| * \left( \cos \left\langle \frac{1}{n_L} \sum_{i=1}^{n_L} \vec{h}_{Li}, \frac{1}{n_R} \sum_{i=1}^{n_R} \vec{h}_{Ri} \right\rangle + \sigma \right) \right) \quad (2.8)$$

According to Equation (1.2), the disparity of local areas with continuous height values is also continuous. Therefore, the disparity values solved in the window are close to the disparity of the central point in the window, and their average can be used as reference disparity  $d_{ref}$  to evaluate the credibility of the disparity of the central point in the window. Based on  $d_{ref}$ , the disparity similarity measurement can be obtained by Equation (2.9).

$$C_{dis} = \frac{x_L - x_R - d_{ref}}{\beta_0 + n * \Delta\beta}, \text{ where } d_{ref} = \begin{cases} \frac{\sum_{i=1}^n d_i}{n} & \text{if } \exists \text{ subpixels } x_1, x_2, \dots, x_n \in N(p) \\ \lambda(x_L - x_R) & \text{else} \end{cases} \quad (2.9)$$

where  $N(p)$  represents a window centered at  $p$  and  $n$  represents the number of boundary points in  $N(p)$ ;  $x_L$  and  $x_R$  represent the x-coordinates of the left and right pixels to be matched, respectively;  $\lambda$  is a scale factor, which determines the relative value of the reference disparity  $d_{ref}$  when no matched pixels exist in  $N(p)$ .  $\beta_0 + n * \Delta\beta$  represents the credibility of the reference disparity: The more matched points in the window, the higher the credibility of the reference disparity  $d_{ref}$ .

To comprehensively consider the shape, gradient and disparity features of the boundary pixels, the above three similarity measurements are weighted and summed up to obtain a multi-similarity measurement fusion like Equation (2.10) shows.

$$S(p, d) = \alpha C_{SSD} + \beta C_{dir} + \gamma C_{dis} \quad (2.10)$$

where  $\alpha$ ,  $\beta$  and  $\gamma$  are the coefficients that control the relative importance of three similarity measurements. The multiple possible values of each coefficient are combined according to the orthogonal table, and the optimal parameter combination is obtained by comparing and analyzing the corresponding experimental results of each combination. For a pixel in the left image, the multi-similarity measurement is calculated for each pixel on the same line in the right image. The "Winner Take All" strategy (WTA) is adopted: the pixel with the smallest multi-similarity measurement is selected as the corresponding matching pixel and the disparity of pixel  $p$  can be obtained as  $d = \arg \min_d S(p, d)$ .

## 2.4 A Flatness Detection Algorithm

Flatness is defined as the maximum height difference  $H$  between the part and the plane supporting it. Refer to Figure 7, for small thin-objects like metal covers, warpage is mainly divided into two forms: bending and twist. For either type of warpage, the highest point on the warped part belongs to the boundary of the part. Therefore, the flatness of a part can be measured as the largest normal distance from all boundary points to the support plane.

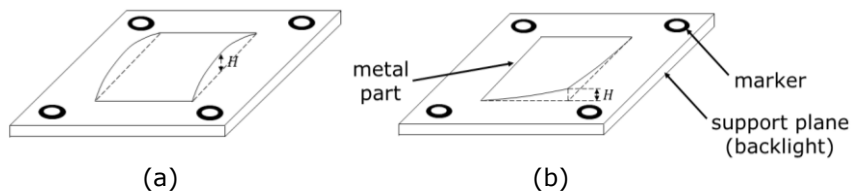


**Figure 7:** Two major types of warpages: (a) bending, (b) twist.

Here we use a flat plane with backlight source as the support plane. Before detecting the flatness, we need to calibrate the plane in order to obtain its space coordinates in the camera coordinate system. For this purpose, refer to Figure 7 and Figure 8, we use a set of special markers whose material is light-transmissive. The inner circle is transparent, and the annular area is covered with a black opaque coating. The design of concentric circles can increase the extraction accuracy of the center of the circle. It should be noted that only once calibration of support plane is needed before the detection of a batch of parts.

In order to calibrate the support plane (backlight), we need to obtain the spatial coordinates  $m_i = [x_i, y_i, z_i]^T$  of the centers of four markers. To do so, we need to use boundary detection and ellipse fitting algorithms to calculate the image coordinates and then their corresponding spatial coordinates. The details of the two algorithms will be elaborated as follows. Firstly, we need to detect the boundaries of the markers. Notice that the shapes of the boundaries are ellipses in both left and right images. Secondly, we need to substitute the detected boundary points into the elliptic equation and calculate the exact parameters of the elliptic equation by the least square method. Based on the calculated elliptic equation, we can obtain the image coordinates of the centers of the ellipses (markers). Thereafter, the spatial coordinates of the centers of four markers can be calculated by the stereo reconstruction principle as introduced in Section 2.1.

After obtaining the spatial coordinates of the markers, the equation of the support plane can be defined as  $Vr = 1$ , where  $V$  is composed of spatial coordinates of four markers and it is equal



to  $[m_1, m_2, m_3, m_4]^T$ ;  $r$  represents the direction of the normal vector of the support plane and it is equal to  $[r_x, r_y, r_z]^T$ . To obtain the heights of all points w.r.t the support plane along the direction of normal vector,  $r$  need to be calculated first. Conventionally,  $r$  can be derived by using the least square method as shown in Equation (2.11)

$$r_{LS} = \arg \min_r \|Vr - 1\|_2^2 = (V^T V)^{-1} V^T \quad (2.11)$$

Let  $n = r_{LS} / \|r_{LS}\|$  be the normal vector, then the distance  $h_j$  from the  $j$ -th spatial point  $p_j$  to the support plane along the normal vector can be obtained by Equation (2.12).

$$h_j = \frac{1}{4} \sum_{i=1}^4 v_{ij}^T n, \quad i = 1, 2, 3, 4 \quad (2.12)$$

where  $v_{ij} = p_j - m_i$  represents the vector from spatial point  $p_j$  to the  $i$ -th marker.

After obtaining the height information of all points w.r.t the support plane, the judgement of the flatness of the part can be measured by Equation (2.13).

$$I = \begin{cases} 1 & \text{if } \max(h_j) > \sigma_h, j = 1, 2, \dots, N \\ 0 & \text{else} \end{cases} \quad (2.13)$$

where  $I$  is a Boolean valuable that indicates whether the tested part is unqualified,  $N$  is the number of all valid points, and  $\sigma_h$  is a user-defined threshold.

### 3 EXPERIMENTS

To evaluate the accuracy and efficiency of the proposed approach, we conducted an experiment on one part by the laser profiler, the structured light system and our approach, each for 100 times which is shown in Section 3.1. Moreover, to evaluate the stability of our proposed approach in practical applications, we applied our approach to the measurement of 200 different parts in Section 3.2, a comparison with the laser profiler and the structured light system is also provided.

#### 3.1 Measurement Accuracy and Efficiency Experiment

The binocular vision system used for our experiment is shown in Figure 8 and the sparse 3D point cloud of the boundary of the part is shown in Figure 9(a).

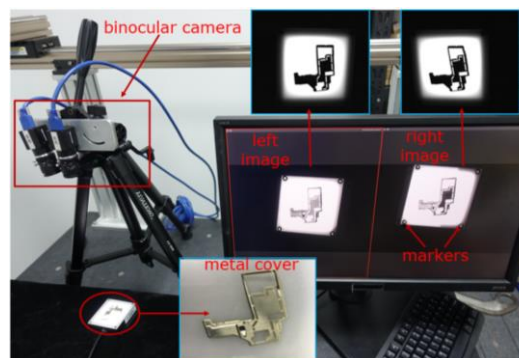


**Figure 8:** The binocular vision system using our proposed 3D boundary reconstruction algorithm.

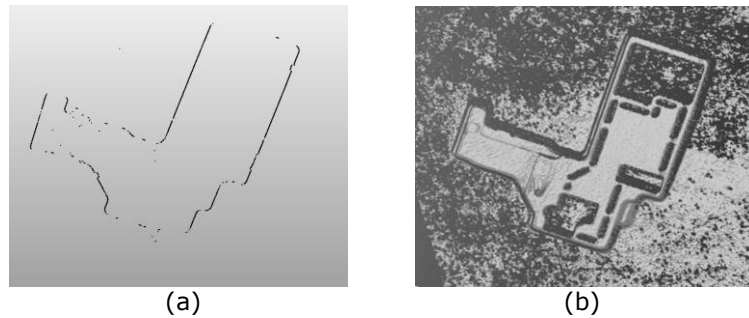


**Figure 9:** (a) The sparse 3D point cloud of the part's boundary reconstructed by our method; (b) the dense point cloud of the part's surface reconstructed by the structured light equipment.

To evaluate the accuracy and efficiency of our proposed approach, using a thin warped metal cover as an example, the laser profiler, structured light system and our proposed approach are compared. As a conventional non-contact measurement method, the laser profiler owns a measuring precision of 0.002mm, but it needs a set of expensive auxiliary mechanisms such as high-precision sliding guides and servo motors. Therefore, we applied the laser profiler to the measurement of the metal cover for 100 times and took the average value as the truth. The hardware required for the three methods are listed as follows.

- Laser profiler: 1\*Laser profiler (KEYENCE LJ-X8060), 1\*High-precision guide rail, 1\*Servo motor (Panasonic MINAS A5 II).
- Structured light system: 2\*Cameras (HIKVISION MV-CE050-30UC), 1\*Projector (TI DLP4500).
- Our method: 2\*Cameras (HIKVISION MV-CE050-30UC), 1\*Backlight (LOTS LTS-FT).

The results of average  $\mu$ , variance  $\sigma^2$  and relative error of each method were obtained by 100 times of repetitive measurements. Meanwhile, to evaluate each method, we summarize the measurement time and cost of the hardwares required in each method in Table 1.

<i>Methods</i>	$\mu(\text{mm})$	$\sigma^2(\text{mm}^2)$	<i>error(%)</i>	<i>time(ms)</i>	<i>hardware cost(\$)</i>
Laser profiler	0.323	8.5e-4	N/A	1280	~8000
Structured light system	0.352	5.6e-3	8.978	1590	~1700
Our method	0.337	3.2e-3	4.334	627	~800

**Table 1:** The accuracy, error, speed and cost of three schemes.

Note: In Table 1, 'N/A' means that the measurement results of the laser profiler are used as the truth.

The results of the experiment reveal that the laser profiler owns the highest measurement precision and smallest variance. However, its hardware cost is significantly higher than the other two methods. More precisely, the laser profiler has the best overall performance, but the cost of this equipment is fairly high (about 5000~10000 dollars).

The structured light system has a relatively high variance and error in the measurement of small metal parts. It needs to project multiple stripes in the reconstruction process, which might induce noises on the boundary due to the refraction light (Figure 9(b)). For smooth and shining object, some special powder is often used to cover on reflective areas to mitigate the reflection problem. But this method is obviously not suitable for the rapid measurement of small metal parts.

The precision of our method is between the precision of the laser profiler and the structured light system. Our proposed method has an obvious advantage in the measurement efficiency. The precision advantage of our method relies on the use of backlight, which makes the boundaries clear and sharp. More importantly, the backlight can avoid the reflection of the metal surface. The speed advantage is due to the following two reasons: (1) the proposed method only needs one shot of the left and the right cameras without using additional operations like projecting multiple stripes; (2) only the boundary of the part is reconstructed. Finally, the proposed method has an obvious advantage in terms of cost and can be regarded as a low-cost choice for flatness measurement in industrial applications.

### 3.2 Measurement Stability Experiment

In order to evaluate the stability of our approach, we further tested 200 different small-sized metal parts using our approach, and compare the measurement results with those of the laser profiler. According to the flatness values, 200 small metal parts are divided into the qualified group and the unqualified group. For ease of computation, we denote by using true positive ( $TP$ ), false positive ( $FP$ ), true negative ( $TN$ ) and false negative ( $FN$ ) as the numbers of the defective unqualified, the defective qualified, the defect-free qualified and the defect-free unqualified parts, respectively. Let  $P_r$  be the ratio of correctly detected unqualified parts w.r.t the total detected unqualified parts; let  $R_c$  be the ratio of correctly detected unqualified parts w.r.t the total real unqualified parts; and let  $A_{cc}$  be the ratio of correct inspection results. They can be expressed as follows:

$$P_r = \frac{TP}{TP + FP}, R_c = \frac{TP}{TP + FN}, A_{cc} = \frac{TP + TN}{TP + TN + FP + FN} \quad (3.1)$$

The flatness detection results for the metal parts are shown in Table 2.

Methods	$P_r$ (%)	$R_c$ (%)	$A_{cc}$ (%)
Laser profiler	100	100	100
Structured light system	96.25	97.47	97.50
Our method	97.50	98.74	98.50

**Table 2:** The flatness detection results for batch metal parts.

In Table 2, the results for the laser profile are all 100% because we take the results of the laser profiler as the truth. Compared with the truth, the vast majority of unqualified parts can be correctly detected and classified by the other two methods. However, according to the flatness detection results, our proposed method is more accurate and stable than the structured light system.

## 4 CONCLUSION

In this paper, we have presented a flatness measurement method for small metal covers (typically less than the size of 2mm\*2mm) based on a binocular vision system. To improve the accuracy and efficiency, we proposed a subpixel boundary detection algorithm based on a hybrid of the Canny operator, Zernike operator and linear interpolation. To solve the mismatching problem of the boundary points on the left and right images, a stereo matching algorithm based on a similarity fusion of shape, gradient and disparity is proposed. To calculate the flatness of the object, we also proposed a calibration method for the support plane (backlight) with specially designed markers.

The experimental results show that the proposed flatness measurement method can achieve excellent accuracy and efficiency. This method has obvious efficiency advantages than the structured light system because it only needs one shot and extracts the boundary information; and the hardware needed in the proposed approach are significantly cheaper compared with the laser profiler scheme. In addition to small metal covers, our proposed method can also be extended to other flatness measurement applications, such as printed circuit board, silicon steel sheets for motors, headset diaphragms and so on.

However, the proposed approach is not universal and has some limitations. In order to ensure nice efficiency, the flatness is measured by reconstructing the bottom boundaries in the proposed approach. In order to make sure that the boundaries are clear and sharp, a backlight source is used to highlight the boundaries, which makes the surface of the object black in images and therefore is not suitable for stereo matching. When the thickness of parts exceeds a threshold (e.g., 5mm), it will induce occlusion or shadow on the boundaries, which will cause non-negligible measurement errors. Therefore, for the parts whose thickness exceeds the threshold, other traditional measurement schemes are still indispensable.

In addition to the flatness measurement, the proposed method can also be used to measure the 3D shape error, and position error of the boundary (including the boundaries of the holes) of thin plate parts efficiently.

#### **Acknowledgement:**

This work is partially supported by the Shanghai International Science and Technology Cooperation Fund No. 18510745700.

Liangang Xie, <https://orcid.org/0000-0002-2887-5154>

Xianda Li, <https://orcid.org/0000-0002-8872-3881>

Xiangzhi Wei, <https://orcid.org/0000-0002-4541-0017>

#### **REFERENCES**

- [1] Aguilar, J. J.; Torres, F.; Lope, M. A.: Stereo vision for 3D measurement: accuracy analysis, calibration and industrial applications, *Measurement*, 18(4), 1996, 193-200. [http://doi.org/10.1016/S0263-2241\(96\)00065-6](http://doi.org/10.1016/S0263-2241(96)00065-6)
- [2] Canny, J.: A computational approach to edge detection, *IEEE Transactions on Pattern Analysis and Machine Intelligence*, 8(6), 1986, 679-698. <http://doi.org/10.1109/TPAMI.1986.4767851>
- [3] Cui, J. W.; Tan, J. B.; Zhou, Y.; Zhang, H.: Improvement of vision measurement accuracy using Zernike moment-based edge location error compensation model, *J. Phys. Conf. Ser.*, 48(1), 2007, 1353-1360. <http://doi.org/10.1088/1742-6596/48/1/252>
- [4] Cui, Y.; Schuon, S.; Thrun, S.: Algorithms for 3D shape scanning with a depth camera, *IEEE Transactions on Pattern Analysis and Machine Intelligence*, 35(5), 2013, 1039-1050. <http://doi.org/10.1109/TPAMI.2012.190>
- [5] Ghosal, S.; Mehrotra, R.: Orthogonal moment operators for sub-pixel edge detection. *Pattern Recognition*, 26(10), 1993, 295-306.
- [6] Guomundsson, S. A.; Pardas, M.; Casas, J. R.: Improved 3D reconstruction in smart-room environments using ToF imaging, *Computer Vision and Image Understanding*, 114(12), 2010, 1376-1384. <http://doi.org/10.1016/j.cviu.2010.07.011>
- [7] Kieu, H.; Pan, T. Y.; Wang, Z. Y.: Accurate 3D shape measurement of multiple separate objects with stereo vision, *Measurement Science and Technology*, 25(3), 2014. <http://doi.org/10.1088/0957-0233/25/3/035401>

- [8] Le, M. T.; Chen, L. C.; Lin, C. J.: Reconstruction of accurate 3-D surfaces with sharp edges using digital structured light projection and multi-dimensional image fusion, *Optics and Lasers in Engineering*, (1)96, 2017, 17-34. <http://doi.org/10.1016/j.optlaseng.2017.04.002>
- [9] Lilienblum, E.; Al-Hamadi, A.: A structured light approach for 3-D surface reconstruction with a stereo line-scan system, *IEEE Transactions on Instrumentation and Measurement*, 64(5), 2015, 1266-1274. <http://doi.org/10.1109/TIM.2014.2364105>
- [10] Marr, D.; Hildreth, E.: Theory of edge detection, *Proceedings of the Royal Society of London*, 207(1167), 1980, 187-217. <https://doi.org/10.1098/rspb.1980.0020>
- [11] Mollada J.; Usamentiaga R.; García D.: On-line flatness measurement in the steel making industry, *Sensors*, 13(8), 2013, 10245–10272. <http://doi.org/10.3390/s130810245>
- [12] Papari, G.; Petkov, N.: Edge and line-oriented contour detection: State of the art, *Image and Vision Computing*, 29(2-3), 2011, 79-103. <http://doi.org/10.1016/j.imavis.2010.08.009>
- [13] Richard, H.; Andrew, Z.: *Multiple View Geometry in Computer Vision*, Cambridge University Press, Canberra, 2004.
- [14] Teague, Reed M.: Image analysis via the general theory of moments, *Journal of the Optical Society of America*, 70(8), 1980, 920-930. <http://doi.org/10.1364/JOSA.70.000920>
- [15] Wang K. C. P.: Elements of automated survey of pavements and a 3D methodology, *Journal of Modern Transportation*, 19(1), 2011, 51–57. <http://doi.org/10.1007/BF03325740>
- [16] Wang, Q.; Kim M. K.; Sohn H.; Cheng J. C. P.: Surface flatness and distortion inspection of precast concrete elements using laser scanning technology, *Smart Structures and System*, 18(3), 2016, 601–623. <http://doi.org/10.12989/sss.2016.18.3.601>